Journal of Magnetic Resonance **148,** 248–256 (2001)
doi:10.1006/jmre.2000.2232, available online at http://www.idealibrary.com on IDEAL®

Site-Selective Electron Nuclear Double Resonance in the Exchange-Narrowed Regime of the ESR in Conducting Solids

G. Denninger,*[,1] K. Baldenhofer,* R. Geßler,* L. Binet,† and D. Gourier†

*2. Physikalisches Institut, Universität Stuttgart, Pfaffenwaldring 57, D-70550 Stuttgart, Germany; and †Ecole Nationale Supérieure de Chimie de Paris, Laboratoire de Chimie Appliquée de l'Etat Solide, UMR CNRS 7574, 11 rue Pierre et Marie Curie, 75231 Paris cedex 05, France

Received March 14, 2000; revised August 2, 2000

Electron nuclear magnetic double resonance on conduction electrons reveals the hyperfine interaction hidden by the fast electron spin exchange. We used the Overhauser shift technique to investigate the electron spin density of the conduction band of gallium oxide, β-Ga_2O_3. Due to the monoclinic structure, the conduction band of β-Ga_2O_3 is anisotropic and it is dominated by contributions from the two nonequivalent Ga sites. The large quadrupole couplings of the two gallium isotopes ^{69}Ga and ^{71}Ga (both with $I = 3/2$) are completely resolved in our double-resonance experiments. This resolved quadrupole interaction allows the determination of the electric field gradients at both gallium sites with high precision and high sensitivity. The resolved quadrupole splitting is the key to the site-selected determination of the hyperfine interaction. The concepts behind these double-resonance techniques are rather general and should be applicable in similar semiconductor systems.

Key Words: **ESR/NMR double resonance; conduction electron spin resonance; hyperfine interaction; electric field gradient determination; site-selective spin density determination.**

INTRODUCTION

Magnetic Resonance in Semiconductors

Recent developments in semiconductor physics have brought up several families of materials such as SiC (*1*), GaN and related alloys (*2*), transparent oxide conductors (TCO) such as ZnO (*3*), and more recently TCOs with rutile type chains (edge-sharing octahedra chains) such as spinels (*4*) or β-Ga_2O_3 (*5, 6*). A better understanding of the relation between the electronic and optical properties of these compounds and their structure requires probing their electronic structure and the atomic environments, especially in the case of TCOs. For these compounds, which contain both unpaired electron spins and nonzero nuclear spins, nuclear magnetic resonance (NMR) and electron spin resonance (ESR) should be natural techniques for such structural investigations. NMR is a high-resolution technique providing geometrical information about atomic sites through the analysis of the electric field gradients (EFGs) but suffers from a low sensitivity. ESR has a much higher sensitivity and detects the conduction electrons, which are the active components of semiconductors. However, the drawback is a low resolution and the hyperfine interaction providing information about the electronic structure and the atomic environments can rarely be analyzed. Electron nuclear double resonance (ENDOR) overcomes these shortcomings. Originally devised by Feher (*7*), ENDOR consists in detecting nuclear spin transitions through a change in the ESR absorption of the electrons interacting with the observed nuclei. This spectroscopy combines the advantages of the high resolution of NMR and the high sensitivity of ESR, along with a great selectivity since only nuclei interacting with unpaired electron spins are detected (*8*). A review of the structural analysis of point defects in solids by ENDOR spectroscopy is given in Ref. (*9*).

As long as the correlation time of an unpaired electron at the nuclear positions is sufficiently long, ENDOR spectroscopy is a powerful technique for determining the hyperfine interactions and the spin density distributions in paramagnetic systems. The spin–spin correlation time τ_c has to be long compared to the inverse hyperfine frequency, $\tau_c \gg h/A_i$, where A_i denotes the hyperfine coupling energy of the nucleus i. This condition is usually fulfilled for localized electronic spins and for large hyperfine couplings A_i. If on the other hand the electronic spin density is distributed over many nuclei, e.g., for a shallow donor electron in semiconductors, the hyperfine couplings A_i become small. By increasing the density n_e of these extended paramagnetic electron states, the exchange interaction of the electronic spins will dominate the paramagnetic properties and the electronic spins will be delocalized. As a consequence, the correlation time τ_c will become fairly short ($\tau_c < 10^{-13}$ s for exchange interactions in the meV range) and the condition $\tau_c \ll h/A_i$ prevails even for large coupling A_i. The ESR line is exchange narrowed with no remaining traces of the hyperfine splitting and ENDOR in the normal way is no longer possible. In fact, the ENDOR lines would be broadened in frequency to something like $\Delta f \approx 1/\tau_c > 10^4$ GHz and are unobservable. The hyperfine interaction $\mathbf{I}_i \cdot A_i \cdot \mathbf{S}$ between the nuclear spin

[1] To whom correspondence should be addressed. E-mail: g.denninger@physik.uni-stuttgart.de. Fax: 0049-711-685-5285.

1090-7807/01 $35.00

$\mathbf{I}_i$ and the electron spin $\mathbf{S}$ is averaged, and the following measurable quantities are observed:

(i) The nuclear resonance position is shifted from the pure Zeeman interaction condition by an effective electronic field $B_e = -A_i \cdot \langle \mathbf{S}_z \rangle / (g_i \mu_n)$, where g_i is the nuclear g factor, μ_n is the nuclear magneton, and $\langle \mathbf{S}_z \rangle$ is the ensemble average of the electronic spin component $\mathbf{S}_z$. The relative shift B_e/B_0 is called the Knight shift in metals, and the paramagnetic shift in semiconductors.

(ii) The electron resonance position is shifted by an effective nuclear field $B_n = A_i \cdot \langle \mathbf{I}_z \rangle / (g_e \mu_B)$, where $\langle \mathbf{I}_z \rangle$ is the ensemble average of the nuclear $\mathbf{I}_z$ component, g_e is the electronic g factor, and μ_B is the Bohr magneton. B_n/B_0 is called the Overhauser shift. In normal metals, the Knight shift is much larger than the Overhauser shift, and the Overhauser shift is very difficult to detect due to the large linewidth of the ESR of the conduction electrons in metals.

Due to the relative sizes of the Knight shift and the Overhauser shift in metals, most hyperfine interaction investigations have been and are done via the Knight shift. This certainly holds for metals, since owing to the large concentration of conduction electrons ($n_e \approx 10^{23}$ cm^{-3}), the Knight shift is rather large and directly accessible. The situation is completely different in systems with a low concentration of paramagnetic electrons, like doped semiconductors: The Knight shift is very small, often below the limit of detection. On the other hand, the nuclear field B_n is proportional to $\langle \mathbf{I}_z \rangle$, and decreasing the temperature will increase $\langle \mathbf{I}_z \rangle$ and thus increase the Overhauser shift. Also, very important experimentally, the nuclear polarization $\langle \mathbf{I}_z \rangle$ can be considerably enhanced by dynamic nuclear polarization (DNP) by partially saturating the ESR transition. The DNP factors obtained in semiconductors are large (a few hundred to up to a few thousand; see details below) and these large enhancement factors enhance the Overhauser shift correspondingly.

Nuclear interactions such as the electric quadrupole coupling are not averaged to zero by the electron spin exchange. The nuclei in the solid at normal conditions do not move from site to site, and thus there is no motional narrowing of the quadrupole interaction. Besides the dipole coupling of the nuclei, the J coupling and possible nuclear couplings via the paramagnetic electrons only lead to a line broadening of the nuclear spin resonance lines of the order of a few kilohertz. If the quadrupole interactions are large compared to these linewidths, they are observable despite the electron exchange processes. In fact, these nuclear interactions are practically not influenced at all by the extended paramagnetic electron state and reflect the values of the solid in the diamagnetic state. Conduction electrons and/or extended shallow donor states at higher concentrations can thus be used to measure nuclear interactions via the electron spin with high sensitivity and high precision (*10, 11*). By detecting the ESR via the luminescence in GaN, the quadrupole splitting of the gallium nuclei was determined in an optically detected ENDOR experiment (*12*). In fact, for systems with a large quadrupole interaction the method is even more attractive than normal high-frequency NMR in the static regime, since the whole spectrum with all the transitions extending over tenths of megahertz can be accumulated in one continuous sweep of the radiofrequency and under magnetic fields much lower than in NMR.

AIM OF THE PAPER

In the experiments communicated here we apply the Overhauser shift technique to investigate single crystals of β-Ga_2O_3. This compound is an n-type semiconductor when slightly oxygen deficient. Slightly in the chemical sense means one vacancy for about 10^4 oxygen atoms. These oxygen vacancies act as shallow donors, and typical electron concentrations are $n_e = 10^{18}$ to 10^{19} cm^{-3}. Several reasons justify the choice of β-Ga_2O_3. First, all the requirements for the double-resonance technique discussed above are fulfilled: The ESR line is exchange or motional narrowed to a linewidth of $\approx$30 μT at room temperature. The ESR resonance is very strong, due to the high number of spins even in tiny single crystals. The overall hyperfine interaction is so large that a bistable ESR response is obtained, manifesting itself by a bistable hysteresis observable even at room temperature (*13–16*). This bistability occurs at sufficiently high microwave fields B_1 (B_1 is the magnetic field component in the rotating frame and is proportional to $\sqrt{P_{\mu w}}$, where $P_{\mu w}$ is the microwave power). This phenomenon is clearly due to the coupling to the nuclei; thus we know that a significant DNP is available even at room temperature. The nuclear interactions are almost exclusively due to the interaction of the electrons with the two gallium isotopes ^{69}Ga and ^{71}Ga (^{69}Ga, $I = 3/2$, 60.1% natural abundance; ^{71}Ga, $I = 3/2$, 39.9% natural abundance). The hyperfine interaction with the oxygen is negligible due to the low natural abundance of only 0.038% for ^{17}O.

The second reason justifying the choice of β-Ga_2O_3 is that its possible applications as TCO in optoelectronics (*6*) as well as the validation of the structural features recognized to explain the bistable ESR (*17, 18*) require some knowledge of the conduction band structure and the environment of the Ga nuclei. This could be provided by the Overhauser shift technique. The last reason is a recent determination of the EFGs by NMR, which was however made difficult by the presence of twins in the large samples used (*19*). These NMR results could be used for comparison with the present investigation. Unlike the case in cubic semiconductors like GaAs or in wurtzite type semiconductors like GaN, the crystal structure of β-Ga_2O_3 is less symmetrical and the EFGs are much larger than, e.g., in GaN. The crystal symmetry of β-Ga_2O_3 is monoclinic, $a = 12.13$ Å, $b = 3.04$ Å, $c = 5.80$ Å, and $\beta = 103.7°$ (*20*). There are two nonequivalent Ga sites in the unit cell. Due to the coordination of the nearest neighbors, these are called tetrahedral site (IV site) and octahedral site (VI site). Note that

the actual site symmetries of the gallium ions are not exactly octahedral or tetrahedral but C_S, with only one mirror plane perpendicular to the *b* axis, and the EFGs are expected to be very different for the two sites.

Due to the low crystal symmetry, the conduction band is expected to be highly anisotropic, and band structure calculations (*17*) and conductivity measurements (*6*) support these expectations: The conduction band edge should mostly be derived from contributions from the Ga VI sites (*15*). This would imply a large hyperfine interaction on the VI site and a small one on the IV site, if the dominant contribution of the interaction was due to *s*-like electrons via a Fermi-contact type interaction $A_i \propto |\Psi(\mathbf{r}_i)|^2$, where $\Psi(\mathbf{r}_i)$ is the electron envelope wavefunction at the nuclear position $\mathbf{r}_i$.

We will show in the following sections that the double-resonance scheme can indeed be used to separate the two sites and the two isotopes unambiguously. This site selection is entirely due to the different EFG tensors at the two sites, and by a complete analysis of the double-resonance quadrupole rotation pattern we obtain the EFG tensors with a precision comparable to that of the recent NMR investigation (*19*). The double-resonance scheme is much more sensitive (the crystal used was smaller by a factor of ≈300 compared to the NMR case) and the problems with crystal twinning seem unimportant (see (*19*) for details), due to the small single crystals which are required. More important is the fact that the hyperfine interaction is now accessible separately for the two sites. This could not be achieved by NMR measurements, since the Knight shift was not observed and is expected to be very small (a few ppm at maximum). Furthermore, there would be problems with a suitable reference for the Knight shift if it were that small.

The double-resonance measurements described below can be extended to supply the individual DNP factors and individual relaxation times for all the transitions. These values could be important for a detailed understanding of the bistable self-organization of the nuclear spins (see (*15, 16*) for details). Here we will concentrate on the complete analysis of the quadrupole pattern, which is a prerequisite for all further double-resonance investigations.

EXPERIMENTAL

The samples were elaborated by the Verneuil method (*21*), which is a melting and recrystallization process enabling the growth of centimeter-size single crystals. The starting powder of Ga_2O_3 (purity 99.99%) was purchased from Metal-Europe. Before the synthesis the powder was heated at 800°C for 8 h to evaporate possible traces of water and carbonates. The crystal growth was performed under slightly reducing conditions with oxygen and hydrogen flow rates of 4.4 and 10.5 l min^{-1}, respectively. The average growth rate was about 1.5 cm · h^{-1}. A 3.2-cm-long single crystal was obtained, with a slight blue color indicating the presence of conduction electrons. Smaller samples with typical size 3 × 0.5 × 0.03 mm could be extracted from this crystal for the ENDOR experiments. Such a small size is necessary to avoid a Dysonian distorsion of the ESR line due to the skin effect.

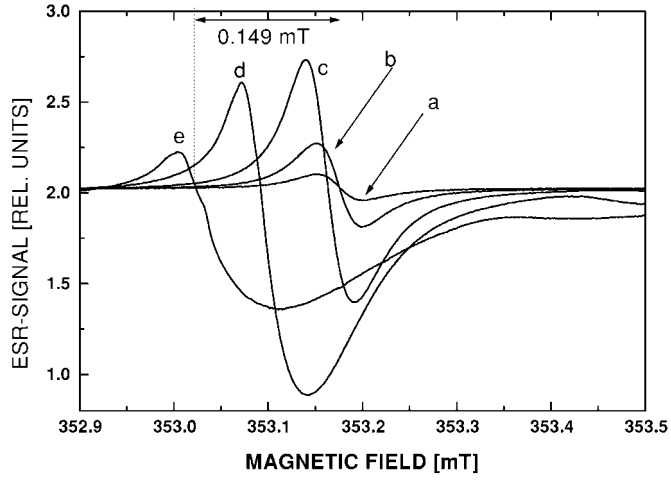

FIG. 1. ESR signal of β-Ga_2O_3 at different microwave powers. $T = 293$ K. (a) 40 dB attenuation; (b) 30 dB; (c) 20 dB; (d) 10 dB; and (e) 2 dB. $P_0 = 200$ mW at 0 dB attenuation.

The basic Overhauser shift experiment consists in measuring the ESR line position with high precision and resolution as a function of a radiofrequency field swept across the region of nuclear transitions. It is essential to lock the field precisely to the center of the ESR transition, since the Overhauser shifts in the present case are as large as the ESR linewidth, and one has to use the special Overhauser lock system described in (*22*).

In contrast to ENDOR experiments, where the use of relatively high radiofrequency power (RF power) is obligatory in order to saturate the hyperfine transitions which have relatively short nuclear T_1 times, Overhauser shift experiments require only low or moderate RF power. Therefore, one can use a standard ESR cavity and insert a double-resonance sample rod. This setup is described in (*10*) and has been used for parts of the experiments described here. The dielectric ENDOR probehead (Bruker, ER4118X-MD5-EN) is a good choice for the Overhauser shift experiments, since the dielectric resonator is practically insensitive to the presence of an electrically conducting sample. The rotation patterns presented below have been conducted with this equipment.

RESULTS AND DISCUSSION

Analysis of the Rotation Patterns

The starting point for an Overhauser shift experiment is the optimization of the ESR resonance. Figure 1 shows spectra recorded in a particular orientation by decreasing the magnetic field. Because of the bistable hysteresis, the lineshape is different when the field is increased. At low microwave power (curve a, −40 dB attenuation, 0 dB = 200 mW) the ESR line is a nearly perfect Lorentzian with $\Delta B \cong 30$ μT. The *g* factor

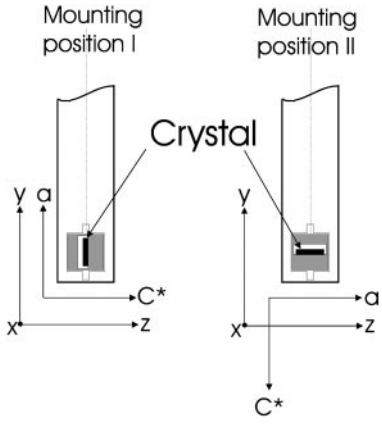

FIG. 2. Schematic drawing of the tip of the ESR sample holder. The material is Vespel. The sample is mounted in the rectangular cut inside a cube. The orientation of the crystal axes are shown for $\varphi_{\mathrm{rot}} = -\varphi_{\mathrm{off}}$. The b axis is along x.

is ≅1.96, depending slightly on the orientation. The g-tensor values and the orientations of the principal axes are known (*23*) and can be used for accurately calibrating the rotation angle offset (see below). Increasing the microwave power not only increases the ESR in amplitude, but clearly shifts the resonance to lower fields and completely changes the lineshape. This behavior is due to the Overhauser shift of all the nuclei and it is exactly the interaction which is studied in detail here. The angular rotation patterns were acquired with the sample mounted in two fixed orientations shown in Fig. 2. For mounting position II, the c^* axis is parallel to the rotation axis y of the goniometer, and the magnetic field $B_0 \| z$ is varied in the a–b plane. The offset of the rotation angle can be calibrated from the known g-tensor values. We used a special mounting procedure of the crystals in a cube of $2 \times 2 \times 2$ mm, which allowed sample reorientations by exactly 90° without remounting the sample.

For both mounting positions double-resonance spectra have been recorded in angular steps of $\Delta\varphi_{\mathrm{rot}} = 10°$ over a complete rotation period of 180°. Figure 3 shows the complete spectra extending from 0 to 20 MHz for one mounting position. The individual spectra are offset along the ordinate for clarity of presentation. We can clearly identify up to about 20 individual shift lines per spectrum extending from practically 0 to about 17 MHz. The highest shift values of individual lines are about 15 μT, and the spectra show a strong angular dependence. The number of shift lines is astonishing at first sight: For $I = 3/2$ one expects three resonance lines with $\Delta m_I = 1$, and with two isotopes ^{69}Ga and ^{71}Ga and the two nonequivalent gallium sites we should have just $2 \times 2 \times 3 = 12$ lines. However, with the rather low Larmor frequencies (about 3.6 MHz for ^{69}Ga and about 4.6 MHz for ^{71}Ga) and the large quadrupole couplings we observe all the six possible transitions in the quadrupole split $I = 3/2$ manifold, and correspondingly can have up to $2 \times 2 \times 6 = 24$ lines. The subsequent analysis of the solutions of the full diagonalization was used to calculate the individual transition rates. All of the transitions in most orientations have sufficiently large transition matrix elements to be excited by magnetic dipole transitions. Note that in this double-resonance scheme we only have to partially saturate the NMR transitions since the observation is done via the electrons. This facilitates the observation of "forbidden" transitions, but we emphasize the fact that these transitions have fairly high transition matrix elements to be excited efficiently in our case.

The interactions responsible for the individual line positions on the frequency axis and for the angular dependence are the quadrupole interaction and the Zeeman interaction. The hyperfine interaction can be completely ignored for the position of the resonance lines in our case. Both from the theoretical model of an extended electron center and from preliminary double-resonance measurements at 94 GHz (W band), we conclude that the Knight shifts are smaller than 5 ppm. This corresponds to $\Delta f_{\mathrm{Knight}} < (4.6\ \mathrm{MHz}) \cdot (5\ \mathrm{ppm}) = 23$ Hz for ^{71}Ga and can be neglected.

We use the following Hamiltonian for a complete analysis of the angular rotation patterns:

$$\hat{H} = -g_{\mathrm{n}} \cdot \mu_{\mathrm{n}} \cdot B_0 \cdot \hat{I}_z + \frac{eQV_{ZZ}}{4I(2I-1)} \times \{3\hat{I}_Z^2 - I(I+1) + \eta \cdot (\hat{I}_X^2 - \hat{I}_Y^2)\}. \qquad [1]$$

The laboratory coordinate system is denoted by x, y, z, and the magnetic field B_0 is along z. The principal axis system of the EFG tensor is denoted by X, Y, Z and the operators $\hat{I}_Z$, $\hat{I}_X$, $\hat{I}_Y$ are along these principal axes, which are different for the two

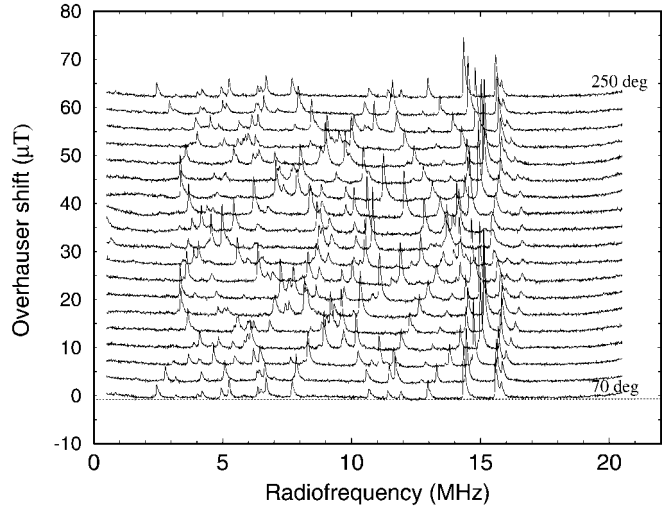

FIG. 3. Rotation pattern of the Overhauser shift of β-Ga_2O_3. Experimental conditions: $T = 293$ K, microwave frequency $f_{\mu w} = 9.6182$ to 9.6188 GHz, $B_0 = 0.34980$ to 0.35026 T, microwave power $P_{\mu w} = 0.159$ W, and $P_{\mathrm{RF}} = 3.25$ W. A fifth-order polynomial background was subtracted for ease of presentation. The successive spectra with $\Delta\varphi = 10°$ are offset by 3.395 μT along the ordinate.

sites. The nomenclature is as usual for the quadrupole interaction: $|V_{YY}| \leq |V_{XX}| \leq |V_{ZZ}|$ and $\eta = (V_{YY} - V_{XX})/V_{ZZ}$ is the asymmetry parameter. The V_{II} ($I = X, Y, Z$) are the electric field gradients along the principal axes, and Q is the electric quadrupole moment of the respective nucleus. The operators $\hat{I}_Z$, $\hat{I}_X$, $\hat{I}_Y$ are transformed to the laboratory system operators $\hat{I}_z$, $\hat{I}_x$, $\hat{I}_y$ by a set of three Euler angles α, β, γ for each site and a common rotation angle φ_{rot} along the y axis. The resulting transformed Hamiltonian is fully diagonalized (C-program routines for the diagonalization of Hermitian matrices, based on procedures described in Ref. (*24*)).

The complete analysis of the rotation pattern from Fig. 3 was done with the following procedure: All the unambiguously identifiable resonance positions f are extracted. At this stage there is no way to assign individual transitions to individual sites or isotopes. The resulting data are a set of resonance positions versus rotation angle φ_{rot}. The model resulting from the Hamiltonian Eq. [1] after the transformation into the laboratory axes system depends on essentially six parameters: B_0, V_{ZZ}, η, and the three Euler angles α, β, γ. B_0 is common to the two sites, and the other five parameters are specific for each site. The two isotopes present no additional complication: once a set of parameters is known for one isotope, it can be carried over to the second isotope by scaling it with the known values of g_n and Q. In the analysis we use $g_n = 1.34439$, $Q = 0.168 \times 10^{-24}$ cm^2 for ^{69}Ga and $g_n = 1.70818$, $Q = 0.106 \times 10^{-24}$ cm^2 for ^{71}Ga. In Fig. 4 we show the resulting fit data for the two sites separately. It is obvious that the model based on Eq. [1] fits the data very accurately and thus unambiguously proves that the quadrupole coupling is responsible for the angular variation. A similar good fit was obtained by analyzing the data from sample mounting position I, and the results are included in Table 1.

The essential parameters obtained by the two experimental data sets are summarized in Table 1. We note that the quadrupole frequencies (eQV_{ZZ}/h) and (eQV_{XX}/h) agree within 0.8% between the two mounting positions. It is not possible to give a reliable statistical error of the individual parameters, since we have only two independent data sets. We estimate a relative accuracy of $\pm 8 \times 10^{-3}$ for the individual quadrupole couplings.

From the Euler angles α, β, γ, and from the known orientations of the crystal axes a, b, c, to the laboratory frame of reference, we can deduce the orientations of the EFG principal axes for the two sites. As b is perpendicular to the a–c mirror plane of the crystal structure, one of the principal axis of both EFG tensors should be along the b direction. Within the estimated errors for the Euler angles this is consistent with our data analysis: For the VI site, the component V_{XX} is along b, and for the IV site it is the component V_{YY}. In the a–c plane we deduce orientations for the principal axes as summarized in Fig. 5. The absolute accuracy of the angles is limited by possible misalignments of the crystal on the sample holder to $\pm 2°$. These errors could be further reduced by aligning the crystals to the sample rod by an *in situ* X-ray analysis. Our data analysis compares very favorably with a similar analysis from NMR experiments (*19*). Table 2 directly compares the essential parameters from both investigations and our assignment of the orientations agrees with that shown in Fig. 3 of Ref. (*19*). Owing to the rather low Larmor frequencies of 3.5 MHz for ^{69}Ga (4.6 MHz for ^{71}Ga) used in this work, we are not able to deduce the chemical shifts of about 200 ppm (IV site) and about 25 ppm (VI site) from our analysis. In fact, these shifts and the reported anisotropies of about 30–40 ppm are so small

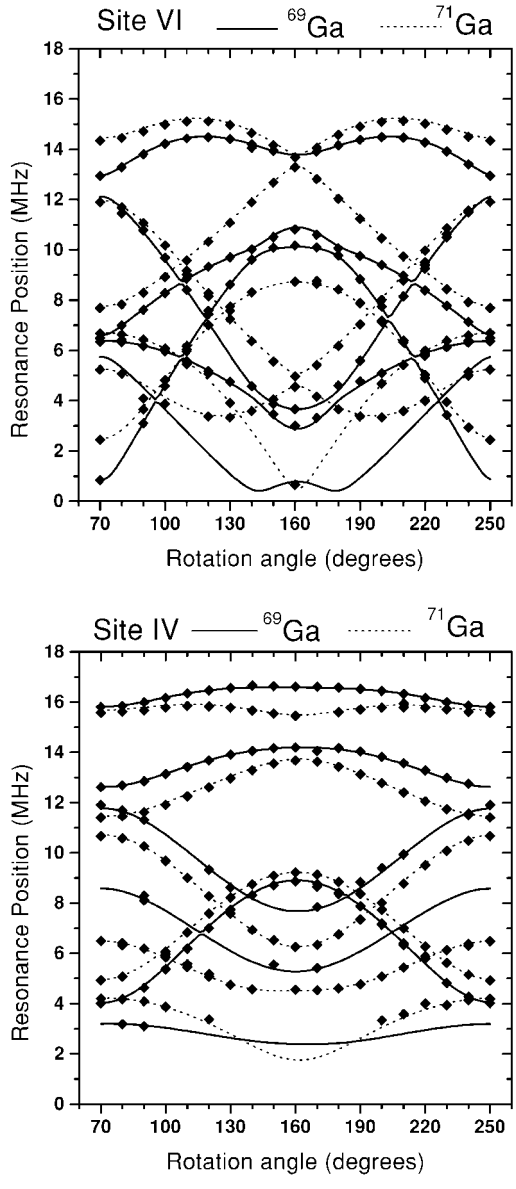

FIG. 4. Comparison of the experimental resonance positions ◆ to the results of the full diagonalization of the Hamiltonian, Eq. [1] (full line, ^{69}Ga; dotted line, ^{71}Ga). The separation into experimental points belonging to the two sites (a, VI site; b, IV site) has been done after the analysis for the purpose of a clear presentation. The extracted parameters are given in the text and in Table 1.

TABLE 1
Parameters from the Rotation Pattern Analysis for the Two Mounting Positions

	Site VI		Site IV	
	Mounting II	Mounting I	Mounting II	Mounting I
$eQV_{ZZ}/(12 \cdot h)$/kHz	1089.46	1085.54	−1356.86	−1352.85
$eQV_{XX}/(12 \cdot h)$/kHz	−594.02	−589.239	1474.36	1471.99
$eQV_{YY}/(12 \cdot h)$/kHz	−495.44	−496.301	−117.5	−119.14
η	0.0905	0.0856	0.8406	0.8381
α/degree	0.16	96.39	3.14	11.38
β/degree	0.05	89.53	9.7	98.05
γ/degree	−2.7	95.95	88.13	97.37

Note. The axes X, Y, Z refer to the reference system oriented by the Euler angles with respect to the laboratory frame x, y, z.

TABLE 2
Comparison of the Data from This Work with NMR Results[a]

Site	Mounting position II	Mounting position I	NMR results[a]
IV			
$C_Q = eQV_{ZZ}/h$/MHz	17.69	17.66	17.71 ± 0.09
η	0.841	0.838	0.854 ± 0.013
VI			
$C_Q = eQV_{ZZ}/h$/MHz	13.07	13.03	13.21 ± 0.08
η	0.091	0.086	0.123 ± 0.012
			0.094 ± 0.008[b]

Note. Only the data for ^{69}Ga are shown; the ^{71}Ga data in our experiment can be scaled by $^{71}Q/^{69}Q$.

[a] Reference (*17*).

[b] From the NMR analysis of the isotope ^{71}Ga.

on our frequency scale that we do not have to include them in our analysis.

DNP Analysis and Site Selection

After the successful analysis of the rotation patterns we are now able to measure double-resonance spectra at any orientation and to unambiguously assign the site, the isotope, and the transition to each observed resonance peak. This enables the calculation of the energy diagram, the occupation differences and the transition matrix elements, and this is a prerequisite for the determination of the individual DNP factors. We now turn to an analysis of the amplitude of an individual Overhauser shift line. Figure 6 depicts a single double-resonance spectrum with $b \| B_0$. The most intense line at 14.33 MHz is enlarged in the inset. The shift amounts to about 12.5 μT and the lineshape is peculiar with a steep rise followed by an apparent exponential decay. This behavior is due to the fact that after saturation in the resonance position, the nuclear polarization can only be built up on the timescale of the nuclear T_1 time. If the transit time Δt_{trans} of the RF sweep through the resonance is not long compared to T_1, these exponential tails appear on the high-frequency sides of all the resonances. Concentrating on one particular line and sweeping the RF so slowly that $\Delta t_{\text{trans}} \gg T_1$, we obtain a nearly pure Lorentzian resonance lineshape, as shown in Fig. 7. The linewidth is about 9.2 kHz and the amplitude depends strongly on the microwave power used to measure the ESR. This directly shows the mechanism of DNP, which results in a higher $\langle I_z \rangle$ when partially saturating the ESR. In fact, the dependence of the Overhauser shift amplitude on the microwave power can be analyzed quantitatively:

$$\Delta B_{\text{ov}} = \Delta B^0_{\text{ov}} \cdot (1 + V \cdot s_{\mu w}). \qquad [2]$$

ΔB_{ov} is the measured Overhauser shift with DNP and ΔB^0_{ov} is the shift in thermal equilibrium at temperature T. The quantity $s_{\mu w}$ is the microwave saturation parameter

$$s_{\mu w} = \frac{\langle \hat{S}_z \rangle^0 - \langle \hat{S}_z \rangle}{\langle \hat{S}_z \rangle^0}, \qquad [3]$$

where $\langle \hat{S}_z \rangle$ is the ensemble average of the electron spin polarization and $\langle \hat{S}_z \rangle^0$ is this value in thermal equilibrium. The ESR transition rate is proportional to $(g_e \mu_B B_1)^2$ and thus propor-

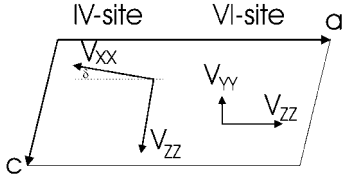

FIG. 5. Principal axes of the EFG tensor in the a–c plane. The third axis is along the b direction perpendicular to the plane. The angle $\delta = 9.7° \pm 3°$. The length of the arrows is proportional to the field gradient.

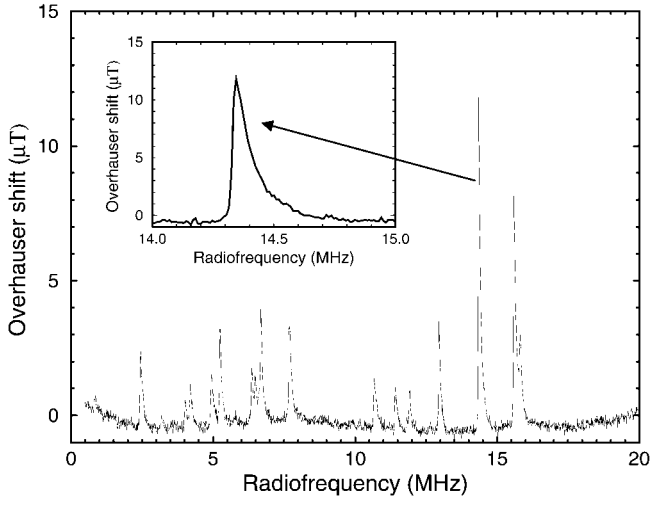

FIG. 6. Overhauser shift spectrum for $b \| B_0$, $\varphi_{\text{rot}} = 250°$, mounting position II. Inset: Enlarged region of the highest shift peak at 14.33 MHz.

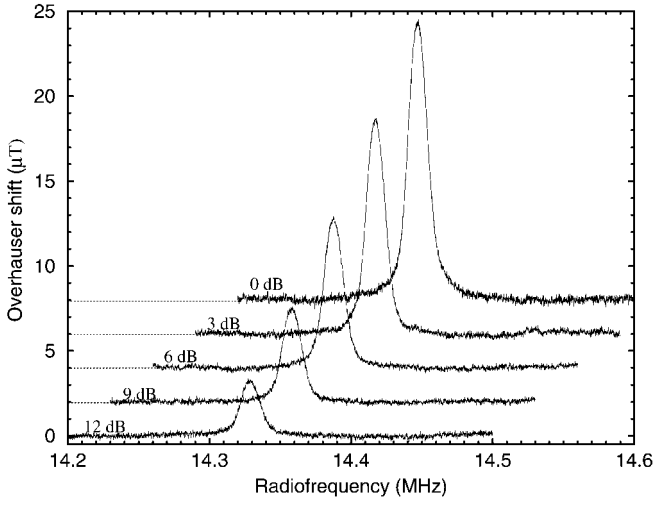

FIG. 7. Dependence of the shift peak at 14.33 MHz on the microwave power. All the other conditions like P_{RF} are fixed. The spectra are offset along the frequency axis and along the ordinate for a clear presentation.

tional to $(g_e\mu_B)^2 P_{\mu w}$ with the microwave power $P_{\mu w}$. The ESR saturation will depend on $P_{\mu w}$ as $s_{\mu w} = \beta \cdot P_{\mu w}/(1 + \beta \cdot P_{\mu w})$, where the parameter β includes $(g_e\mu_B)^2$ and the cavity-dependent relation between B_1^2 and $P_{\mu w}$, so that Eq. [2] is reformulated as

$$\Delta B_{ov}(P_{\mu w}) = \Delta B_{ov}^0 \cdot \left(1 + V \cdot \frac{\beta P_{\mu w}}{1 + \beta P_{\mu w}}\right). \qquad [4]$$

From a fit of the amplitudes of the Overhauser shift from Fig. 7 to Eq. [4] one can deduce the three parameters ΔB_{ov}^0, V, and β. Plotting ΔB_{ov} versus $s_{\mu w} = \beta \cdot P_{\mu w}/(1 + \beta \cdot P_{\mu w})$, one obtains a linear relation as shown in Fig. 8. The behavior of this Overhauser shift line is as expected for a DNP situation. Note that the fit is not particularly sensitive to the individual parameters ΔB_{ov}^0 and V, if $V \gg 1$. In this case, only the product $\Delta B_{ov}^0 \cdot V$ is reliably determined. In order to obtain ΔB_{ov}^0 and V separately, one has to measure ΔB_{ov} with high precision at such low microwave power that the product $V \cdot s_{\mu w}$ is close to 1.

The Overhauser shift relies on the nearly complete saturation of the NMR transitions. Of course complete saturation $s_{RF} = 1$ cannot be obtained, since this would considerably broaden the NMR transition. But the extrapolation to $s_{RF} \to 1$ can be done very reliably by measuring ΔB_{ov} at fixed microwave power $P_{\mu w}$ and varying the radiofrequency power P_{RF}. Again, the RF saturation is $s_{RF} = \beta_{RF} \cdot P_{RF}/(1 + \beta_{RF} \cdot P_{RF})$, with a suitable parameter β_{RF}. A fit to the relation

$$\Delta B_{ov}(P_{RF}) = \Delta B_{ov}^{\infty} \cdot \frac{\beta_{RF} \cdot P_{RF}}{1 + \beta_{RF} \cdot P_{RF}} \qquad [5]$$

is sufficient to extrapolate to the value ΔB_{ov}^{∞} for complete RF saturation. This is shown in the inset of Fig. 8 for the value at $P_{\mu w} = 100$ mW (3 dB microwave attenuation). This extrapolation to $s_{RF} \to 1$ has to be done separately for every NMR transition, since it depends on the individual relaxation times T_1. Fortunately, this extrapolation does not depend on the DNP and thus does not depend on $P_{\mu w}$. This allows one to do this extrapolation for one fixed $P_{\mu w}$, and then scale all the appropriate values.

The results of the full analysis are ΔB_{ov}^0 and V for each NMR transition. As $\Delta B_{ov}^0 = A \cdot \langle \hat{I}_z \rangle^0/(g_e\mu_B)$ we can determine the hyperfine interaction A, since the thermal equilibrium polarization $\langle \hat{I}_z \rangle^0$ can be calculated. Under the assumption of a dominant Fermi-contact type interaction,

$$A = \frac{8\pi}{3} \cdot \frac{\mu_0}{4\pi} \cdot (g_e\mu_B) \cdot (g_n\mu_n) |\Psi(0)|^2, \qquad [6]$$

the spin density at a nuclear site $|\Psi(0)|^2$ is thus directly accessible. And since this analysis can be done selectively for transitions of the two different sites, the contribution of this particular site to the conduction band wavefunction can be determined. Experiments along these lines are under way and a preliminary analysis shows a higher value of ΔB_{ov}^0 resulting from the VI site. However, the ΔB_{ov}^0 values at $T = 300$ K are very small and quantitative results on the band structure require further data sets at lower T.

CONCLUSIONS

We have shown that even in the regime of complete exchange and/or motional narrowing the hyperfine interaction can still be obtained and resolved for the different sites by using the double-resonance technique Overhauser shift spec-

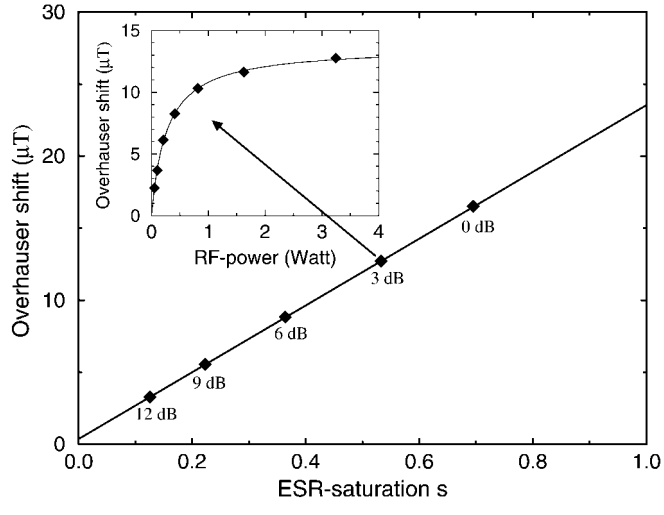

FIG. 8. Analysis of the dynamic nuclear polarization. The shift data are plotted versus the ESR saturation parameter s. Details of the procedure are in the text, and the fit values are $\Delta B_{ov} = 0.362\ \mu T \cdot (1 + 64.06 \cdot s)$. Inset: Dependence of the shift peak at $P_{\mu w} = 3$ dB on the radiofrequency power P_{RF}. The line is a fit to the RF saturation: $\Delta B_{ov} = 13.69\ \mu T \cdot 3.76\ W^{-1} \cdot P_{RF}/(1 + 3.76\ W^{-1} \cdot P_{RF})$.

troscopy. The key to the success is the fact that pure nuclear interactions like the electric quadrupole interaction are not influenced by the paramagnetic electrons. The quadrupole splitting in fact labels the NMR transitions to the different sites, and the amplitude of the Overhauser transitions is proportional to the hyperfine coupling. In contrast to previous applications in GaN and ZnO (Ref. (*10*)), there are two nonequivalent gallium sites in β-Ga_2O_3, and these can be separated by the quadrupole interaction. Spectral diffusion in the nuclear system between the two sites is small due to the large quadrupole splitting. Thus the two sites are accessible individually. This is essential for the site-selective determination of the hyperfine interaction. In fact, this is the first example where such a site selection of the hyperfine interaction was possible in an exchange-narrowed system. From the analysis of the resonance frequency positions, one obtains the EFG tensor values and the principal axis orientations with a precision similar to that of NMR investigations. One can use considerably smaller single crystals than for NMR due to the much higher sensitivity. The accuracy of the EFG parameters is comparable to that of the NMR investigation. In addition the Overhauser shift technique has access to all the transitions and, e.g., inhomogeneous distributions of the EFGs would be reflected in different linewidths of the individual transitions. However, a careful set of high-precision measurements is necessary to extract quantities like ΔB^0_{ov} and V, as outlined above. Due to its high sensitivity and high selectivity, ENDOR by the Overhauser shift technique in conducting solids could be a very efficient tool for investigating systems containing a very small number of nuclear spins such as thin layers or interfaces.

Possible extensions are straightforward, but require more sophisticated double-resonance equipment: The time dependence of the Overhauser shift of the individual lines can be measured giving the individual T_1 times and the DNP enhancement factor $V = f(g_e\mu_B)/(g_n\mu_n)$, where f is the leakage factor. This leakage factor f depends on the relaxation rate via the paramagnetic electrons compared to other relaxation channels, $f = w_e/(w_e + w_0)$, where w_e and w_0 are the relaxation rates by the electrons and by other processes, respectively. Since $(w_e + w_0) = 1/T_1$, a measurement of V and T_1 allows one to quantitatively disentangle the relaxation processes. This is the only reliable way to separate w_e and w_0 and can be done as a function of temperature.

Going to higher ESR frequencies will increase $\Delta B^0_{ov} \propto f_{\mu w}$ and one approaches the high-field condition with 10 times higher Larmor frequencies up to 45 MHz at a microwave frequency $f_{\mu w} = 94$ GHz. Experiments in a recently constructed double-resonance cavity at 94 GHz are under way in our laboratory. However, rotations of the crystals along an axis perpendicular to B_0 are not possible in the Fabry–Perot setup used in our experiments at 94 GHz. Commercial cylindrical ENDOR resonators at 94 GHz became available only very recently. These would allow the rotations of the single crystals and double-resonance investigations at high ESR/NMR frequencies.

ACKNOWLEDGMENTS

Experimental contributions from double-resonance experiments at $f_{\mu w} = 94$ GHz by H.-J. Kümmerer and K. Hüftle helped to clarify the quadrupole splitting.

REFERENCES

1. J. B. Casady and R. W. Johnson, Status of silicon carbide (SiC) as a wide-bandgap semiconductor for high-temperature applications: A review, *Solid-State Electron.* **39,** 1409–1422 (1996).
2. S. P. Denbaars, Gallium-nitride-based materials for blue to ultraviolet optoelectronics devices, *Proc. IEEE* **85,** 1740–1749 (1997).
3. V. A. Nikitenko, Luminescence and EPR of zinc oxide, *J. Appl. Spectrosc.* **57,** 783–798 (1992); D. Reiser, J. Blömker, G. Denninger, and J. Schneider, A magnetic double-resonance investigation of the quadrupole interaction in ZnO single crystals, *Solid State Commun.* **102,** 359–363 (1997).
4. T. Moriga, T. Sakamoto, Y. Sato, A. H. Khalid, R. Suenari, and I. Nakabayashi, Crystal structures and electrical and optical properties of $MgIn_{2-x}Ga_xO_4$ solid solutions, *J. Solid State Chem.* **142,** 206–213 (1999); H. Kawazoe, N. Ueda, H. Un'no, T. Omata, H. Hosono, and H. Tanoue, Generation of electron carriers in insulating thin film of $MgIn_2O_4$ spinel by Li^+ implantation, *J. Appl. Phys.* **76,** 7935–7941 (1994); T. Omata, N. Ueda, K. Ueda, and H. Kawazoe, New ultraviolet-transport electroconductive oxide, $ZnGa_2O_4$ spinel, *Appl. Phys. Lett.* **64,** 1077–1078 (1994).
5. J. M. Phillips *et al.,* Transparent conducting thin films of $GaInO_3$, *Appl. Phys. Lett.* **65,** 115–117 (1994).
6. N. Ueda, H. Hosono, R. Waseda, and H. Kawazoe, Anisotropy of electrical and optical properties in β-Ga_2O_3, *Appl. Phys. Lett.* **71,** 933–935 (1997).
7. G. Feher, Electron spin resonance experiments on donors in silicon. I. Electronic structure of donors by the electron nuclear double resonance technique, *Phys. Rev.* **114,** 1219–1244 (1959).
8. J. R. Niklas and J.-M. Spaeth, Application of ENDOR-induced electron spin resonance to the study of point defects in solids, *Phys. Status Solidi B* **101,** 221–231 (1980).
9. J.-M. Spaeth, J. R. Niklas, and R. H. Bartram, "Structural Analysis of Point Defects in Solids," Springer Series in Solid-State Sciences, Vol. 43, Springer-Verlag, Berlin (1992).
10. G. Denninger and D. Reiser, Determination of electric-field gradients in semiconductors with high precision and high sensitivity, *Phys. Rev. B* **55,** 5073–5078 (1997).
11. G. Denninger, R. Beerhalter, D. Reiser, K. Maier, J. Schneider, T. Detchprohm, and K. Hiramatsu, Shallow donors in GaN: A magnetic double resonance investigation, *Solid State Commun.* **99,** 347–351 (1996).
12. F. K. Koschnick, K. Michael, J.-M. Spaeth, B. Beaumont, and P. Gibart, Optical detection of electron nuclear double resonance on a residual donor in wurtzite GaN, *Phys. Rev. B* **54,** R11042 (1996).
13. E. Aubay and D. Gourier, Bistability of the magnetic resonance of conduction electrons in gallium oxide, *J. Phys. Chem.* **96,** 5513–5520 (1992).
14. E. Aubay and D. Gourier, Magnetic bistability and Overhauser shift of conduction electrons in gallium oxide, *Phys. Rev. B* **47,** 15023–15036 (1993).
15. D. Gerbault and D. Gourier, Bistable self-organization of nuclear spins in conducting solids, *Phys. Rev. B* **54,** 6315–6326 (1996).
16. D. Gourier, L. Binet, and D. Gerbault, Hysteresis and memory of the magnetic resonance of conduction electrons in solids. From bist-

ability to stochastic resonance, *Appl. Magn. Reson.* **14,** 183–201 (1998).

17. L. Binet, D. Gourier, and C. Minot, Relation between electron band structure and magnetic bistability of conduction electrons in β-Ga_2O_3, *J. Solid State Chem.* **113,** 420–433 (1994).
18. L. Binet and D. Gourier, Bistable magnetic resonance of conduction electrons in solids, *J. Phys. Chem.* **100,** 17630–17639 (1996).
19. T. Vosegaard, I. P. Byriel, L. Binet, D. Massiot, and H. J. Jakobsen, Crystal structure studies by single-crystal NMR spectroscopy. ^{71}Ga and ^{69}Ga single-crystal NMR of β-Ga_2O_3 twins, *J. Am. Chem. Soc.* **120,** 8184–8188 (1998).
20. S. Geller, Crystal structure of β-Ga_2O_3, *J. Chem. Phys.* **33,** 676–684 (1960).
21. M. Ueltzen, The Verneuil flame fusion process: Substances, *J. Cryst. Growth* **132,** 315–328 (1993).
22. G. Denninger, "Overhauser Shift" Experiments with Conventional ENDOR-Equipment, Bruker Report No. 1/1987, pp. 18–21 (1987).
23. L. Binet and D. Gourier, Origin of the blue luminescence of β-Ga_2O_3, *J. Phys. Chem. Solids* **59,** 1241–1249 (1998).
24. W. H. Press, S. A. Teukolky, W. T. Vetterling, and B. P. Flannery, "Numerical Recipes in C," 2nd ed., Cambridge Univ. Press, Cambridge (1995).